Cellulose (2025) 32:10469–10489
https://doi.org/10.1007/s10570-025-06824-0

ORIGINAL RESEARCH

The role of cation and anion on the dissolution rate of flax yarns in ionic liquids

Fatimah A. Albarakati · Peter J. Hine · Michael E. Ries

Received: 14 March 2025 / Accepted: 16 October 2025 / Published online: 31 October 2025

Abstract This study investigates the dissolution of flax yarns in two imidazolium based ionic liquids ILs (1-butyl-3-methylimidazolium acetate) ($[C4mim]^+[OAc]^-$), and (1-ethyl-3-methylimidazolium octanoate) ($[C2mim]^+$ $[Oct]^-$). These results are combined with our previous published work on (1-ethyl-3-methylimidazolium acetate) ($[C2mim]^+[OAc]^-$) (Albarakati et al.2023) using the same flax yarns, to establish an understanding of the effect of the anion and cation on dissolution behaviour. The dissolution process involved submerging the flax yarns in the ILs for a range of temperatures and times, followed by coagulation in water. The dissolved coagulated material produced an outer ring that surrounded the centre undissolved yarn. Optical microscopy was used to follow the growth of this region, which was found to follow an Arrhenius behaviour. The dissolution activation energies of the ILs [C4mim][OAc] and [C2mim] [Oct] were found to be 67 ± 1 kJ/mol and 79 ± 1 kJ/mol, respectively. In addition, the growth of the outer coagulated ring's thickness was measured with time and temperature, enabling the IL's diffusion to be determined. Nuclear Magnetic Resonance, viscosity and density measurements were combined through a Stokes–Einstein analysis to further understand the dissolution mechanisms. Comparing the resultant data for all three ILs shows that the dissolution rate goes from fastest to slowest in the order [C2mim][OAc] > [C4mim][OAc] > [C2mim][Oct]. Our key observation is that the dissolution of the flax yarns (in all three ILs) is controlled by the diffusion of each IL through a region of swollen cellulose/IL solution around each yarn as it dissolves.

Keywords Cellulose · Dissolution · Time–temperature superposition · Activation Energy · Ionic liquids · [C2mim][OAc] · [C4mim][OAc] · [C2mim][Oct]

Supplementary Information The online version contains supplementary material available at https://doi.org/10.1007/s10570-025-06824-0.

F. A. Albarakati
Department of Physics, University of Umm Al-Qura, P.O. Box 56335, 21955 Makkah, Saudi Arabia
e-mail: fabarakati@uqu.edu.sa

P. J. Hine · M. E. Ries (✉)
School of Physics and Astronomy, University of Leeds, Woodhouse Lane, Leeds LS2 9JT, UK
e-mail: m.e.ries@leeds.ac.uk

P. J. Hine
e-mail: p.j.hine@leeds.ac.uk

Introduction

Lignocellulose, which includes cellulose, hemicellulose, and lignin have great potential as renewable raw materials with an annual production of around 10^{11} tons per year (Li et al. 2018). Cellulose is a key component of plant cell walls found in

trees, plants, and algae with 40 billion tons of renewed annually (Olivier-Bourbigou et al. 2010), so cellulose is considered a promising feedstock for the development of sustainable materials (Reddy and Yang 2005; Wang et al. 2016). It is widely acknowledged that the breakup of the intra- and intermolecular hydrogen bonds in cellulose is the crucial point in the dissolution of this polymer (Bochek 2003). Since cellulose does not dissolve in common solvents, such as water, there has been a need to find alternative solvents. Ionic liquids (ILs) have a huge potential to be 'green' solvents for dissolving cellulose and making all cellulose composites (Soykeabkaew et al. 2009; Tanpichai et al. 2022), due to their notable excellent properties including the ability to dissolve cellulose without any pretreatment (Swatloski et al. 2002). ILs are organic salts and have a melting point below 100 °C (Vilaro et al. 2024), low vapor pressure, high thermal stability, and recyclability (Miao and Hamad 2013). The dissolution mechanism of cellulose is not fully understood, even though it is a crucial stage in the processing of cellulose, which occurs prior to its transformation into high-value products through the use of anti-solvents for coagulation (Ju et al. 2022). The dissolution of cellulose occurs predominantly through the interaction between the anion of the IL with the hydrogen atoms of the hydroxy groups of cellulose whilst the cation associates with the oxygen atoms of the hydroxy groups (Feng and Chen 2008). After dissolution comes a coagulation process which includes two steps: the first is when the solvent has been sufficiently removed by a suitable anti-solvent, in this case water, then followed by a drying process.

Previously reported literature has suggested that the IL anion mostly controls the dissolution of cellulose (Cho et al. 2011; Lu et al. 2014; Zhang et al. 2016; Zhao et al. 2013). The anions activity highly depends on their charge, size, and polarity while dissolving (Bonifacio et al. 2023). The dissolution rate of 1-ethyl-3-methylimidazolium ($[C_2C_1Im]$) in different ionic liquids (ILs) was investigated by Villar et al. (2023) with a focus on various anions, including acetate ([OAc]), diethyl phosphate ([DEP]), and dimethyl phosphate ([DMP]). They found that [OAc] significantly increases the rate of the dissolution compared to [DEP] or [DMP]. This enhanced dissolution efficiency was attributed to the strong interaction between [OAc] and cellulose, which effectively disrupts the hydrogen-bond network. Consequently, the results demonstrate that the dissolution rate of cellulose in ILs is highly dependent on the type of the anion (Villar et al. 2023). The interaction between anion and cellulose made up of glucose units holds great interest. The glucose chains in cellulose are held together by hydrogen bonds, these bonds are important in maintaining the material's strength and stability (El Seoud et al. 2021). There have been investigations reported previously on anion chain lengths of $m = 0$–3, where m represents the alkyl chain length of anion: formate ($[HCOO]^-$) ($m = 0$), acetate ($[CH3COO]^-$) ($m = 1$), propionate ($[CH3CH2COO]^-$) ($m = 2$), butyrate ($[CH3(CH2)2COO]^-$) ($m = 3$) (Xu et al. 2010, 2012, 2014). However, to the best of our knowledge, no solubility experiments with cellulose and the [Oct] group has been investigated. The octanoate $[Oct]^-$ anion with the longer chain length of $m = 8$ would be expected to influence the dissolution process in the similar way by disrupting the H-bonds. A molecular dynamic study by Hua et al. (2024) reported that shorter alkyl chains reduce steric hinderance which allow higher efficiency of the interaction between anion and cellulose. While longer chain length increases steric hinderance, decreasing the efficiency of the interaction (Hua et al. 2024). Therefore, the H-bond is harder to form in the longer alkyl chain, making the cellulose hard to dissolve (Xu et al. 2015; Zhao et al. 2012).

Most researchers acknowledge the role of cation in the solubility of cellulose as only secondary and that their function remains less significant compared to the anions, nevertheless it is imperative for one not to dismiss its role. A review of various research works indicates a weaker interaction between cations and cellulose in the dissolution (Fernandes et al. 2011; Gupta and Jiang 2015; Klähn et al. 2011; Ocreto et al. 2022). Researchers such as Lu et al. (2014) noted that the interaction between the imidazolium cation and glucose rings occur through the actions of van der Waals interactions. Furthermore, the need to understand the complex interactions between cellulose and cations remains valid for a detailed review of the mechanisms for cellulose solubility. A study by Mezzetta et al. (2019) investigated the significant changes in the ILs solubility power after various cations are combined with the anion. They also examined the cation characteristics, with a focus on the alkyl chain

length for the charge-carrying component of the cation (Mezzetta et al. 2019). Extensive research by Zhao et al. (2012) investigated the effect of cationic structures on cellulose dissolution in ionic liquids. A simulation was performed by the authors for a variety of chloride based ILs that were attached on imidazolium and pyridium and contained alkyl chains of varying lengths. In addition, this investigation examined the dissolution of cellulose in [C4mpy]Cl (Butyl-3-Methylpyridium Chloride) and 1-butyl-3-methylimidazolium chloride [C4mim]Cl. It was determined that [C4mpy]Cl dissolves cellulose more effectively than [C4mim]Cl. The findings were significant as they demonstrated that IL [C4mpy] with shorter alkyl chains have a greater ability to dissolve cellulose compared to those with longer chains [C4mim] (Zhao et al. 2012). The research also explored the effect of incorporating an electron-withdrawing group within the alkyl chain of the cation using AMIM+, which was adopted as a model that demonstrated the electron-withdrawing group present within the alkyl chain of the cation led to more enhanced interactions between the cellulose and the cation as result, the interactions led to more dissolution efficiency for the cellulose. Furthermore, they demonstrate the value and role of alkyl chain characteristics, cationic properties, and electron-withdrawing groups within the above process. Gaining insight into the cationic structural function can help in the development of ionic liquids that have enhanced ability to dissolve cellulose.

The structure of ionic liquids can have a significant influence on cellulose processing due to their capacity to disrupt the strong hydrogen bond network that forms between polymer chains. The first studies on IL-cellulose interactions mainly looked at 1-alkyl-3-methylimidazolium [C_n mim] cations with chain lengths from 4 to 8 and different anions. They found that [C_n mim] Cl (with $n=4$) was the most efficient in increasing the dissolution rate among the ILs tested (Moulthrop et al. 2005; Swatloski et al. 2002; Zhang et al. 2005). Another study demonstrated that the properties of the IL and its capacity to dissolve cellulose were significantly influenced by the length of the cation side chain (Roy and Rodgers 2021). ILs that contained different [C_n mim]$^+$ cations evidenced that the solubility of these ILs was influenced by the length of the cation chain, specifically demonstrating an odd–even effect. Interestingly, the ILs with a chain length as order of [C_6 mim]$^+$ < [C_4 mim]$^+$ < [C_2 mim]$^+$ exhibited the highest solubility among a range of anions (Erdmenger et al. 2007; Roy and Rodgers 2020; Vitz et al. 2009). In a related work, they used molecular dynamics calculations to investigate how cellulose dissolves in [$C_n$mim]-based ILs. The patterns of bonding that existed between the cations, anions, and cellulose chains were analysed. At the same time as increasing the length of the cation chain caused the dynamics of the system to slow down slightly, it was discovered that this change had only a marginal impact on the solvation process (Bylin et al. 2014; Rabideau and Ismail 2015).

This current work has involved a fundamental study of the dissolution mechanism of flax yarns in different three ionic liquids shown in Fig. 1, along with a method to measure the dissolution energy (Budtova and Navard 2015; Chen et al. 2020) employed by our research group using time temperature superposition (Albarakati et al. 2023; Alghamdi et al. 2024; Alrefaei et al. 2023; Hawkins et al. 2021; Liang et al. 2021; Zhang et al. 2021). In a previous published paper, we presented a study of the dissolution of flax yarns in 1-ethyl-3-methyl-imidazolium acetate [C2mim][OAc] and developed the methods to determine the dissolution activation energy. It is known than the choice of anion and cation play a crucial role in determining the efficiency of cellulose dissolution by understanding the impact of the ion type, cation/anion combination and size is crucial for creating ILs with specific features. For this reason, the current work presents a study of two further ILs, namely 1-ButyI-3-methylimidazolum Acetate, [C4mim][OAc] and 1-Ethyl-3-methylimidazolium Octanoate [C2mim][Oct]. These were chosen as one of these has the same cation [C2mim] as the previous study and while the other has the same anion [OAc], allowing the effect of the different ion combinations to be compared and contrasted.

Optical microscopy allowed the growth of the dissolved and coagulated fraction at various temperatures and times to be directly measured. An activation energy in cellulose/ILs mixtures is then determined from time–temperature superposition (TTS) of these results. In addition, the growth of the thickness of the outer ring of the coagulated material was investigated over time and temperature, leading to interesting insights into the IL's diffusion coefficients. These measurements

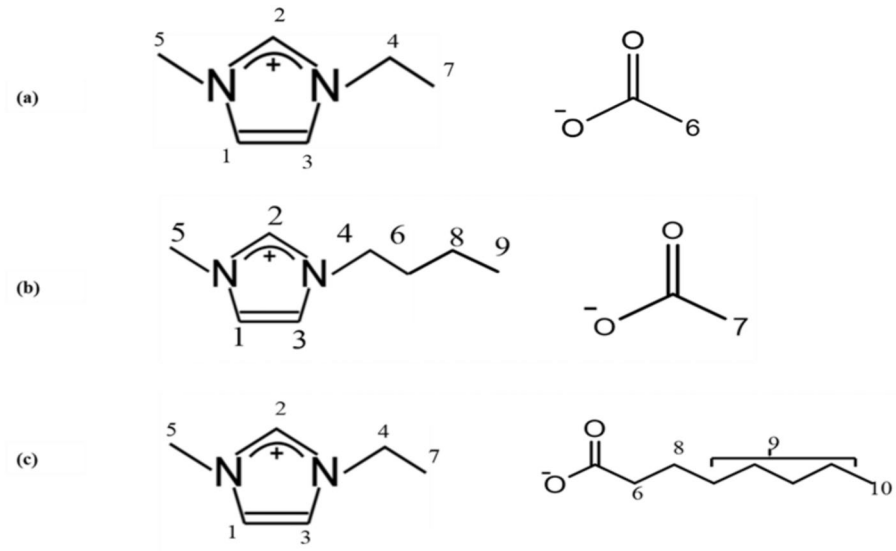

Fig. 1 The three ionic liquids investigated in this study: **a** 1-ethyl-3-methyl-imidazolium acetate $[C2mim]^+[OAc]^-$, **b** 1-ButyI-3-methyl-imidazolum Acetate, $[C4mim]^+[OAc]^-$, and **c** 1-Ethyl-3-methylim-idazolium Octanoate, $[C2mim]^+[Oct]^-$. ^1H NMR resonances are labelled according to the spectral assignment and previous publication by (Green et al.2017; Lefroy et al.2021; Ries et al.2014)

displayed an Arrhenius behaviour, which allowed the measurement of the required activation energy for the dissolution for each of the ILs to be determined. These dissolution processes are complemented by Nuclear Magnetic Resonance (NMR) self- diffusion measurements, density and viscosity measurements to provide further understanding into the underlying dissolution mechanisms. These results were then used to apply the Stokes–Einstein analysis. These findings can provide insightful information for how changing the cation/anion chain length might affect the dissolution behaviour highlighting the need for additional re-evaluation of established mechanisms for cellulose dissolution in ILs which can help on the development and use of ILs on the production of all-cellulose composites using flax fibre such as in films, or other cellulose-derived products.

Experimental

Materials

The cellulose source used in this study was a flax yarn purchased from (Airedale Yarns, Keighley, UK) and was the same as used in the previously published paper using 1-ethyl-3-methyl-imidazolium acetate [C2mim] [OAc] (Albarakati et al. 2023). The material was in the form of a continuous yarn and had a diameter of 0.5 mm. The two new ionic liquids used in this study were 1-buthyl-3-methyl-imidazolium acetate [C4mim][OAc] with a purity of 98%, and 1-ethyl-3-methyl-imidazolium octanoate [C2mim] [Oct] with a purity of 98% which were all purchased from Proionic GmbH, Grambach, Austria. To provide an overall picture of the effect of the anion and cation, some additional experiments (NMR, viscosity and density) were also carried out using the IL from the previously reported study, which was 1-ethyl-3-methyl-imidazolium acetate [C2mim] [OAc] with a purity of 98% also supplied by Proionic GmbH, Grambach, Austria. Epoxy resin was used to embed the samples (Epoxicure, Cold Cure Mounting Resin from Buehler, UK) and then viewed using optical microscopy (OM) in reflection to allow for clear images. An MBraun Labmaster 130 glove box was used to prevent water contamination in the IL samples for NMR and density measurements. Karl-Fischer titration using a Metrohm 899 Coulometer was employed to determine the water content in ionic liquids as received, giving the water content in the experiments of [C2mim][OAc], [C4mim][OAc], and [C2mim][Oct] at 0.2 wt.%, 0 wt.%, and 0.1wt.% respectively.

Preparation methods

The partially dissolving method was used to follow the dissolution for both new ILs [C4mim][OAc] and [C2mim][Oct] which is identical to the method

for the same flax yarns in IL [C2mim][OAc], which is described in our previous paper (Albarakati et al. 2023). A Teflon dish was filled with IL [C2mim][Oct] or [C4mim][OAc] (approx. 50 ml) and preheated at the chosen desired temperature in an oven for 1 h. Four separate yarn samples were wound around a Teflon frame. Then, the frame with the samples was submerged into the preheated IL, the dissolution experiments were then commenced at the various chosen times and temperatures in a vacuum oven under vacuum, after which the frame with samples was taken out from the IL and placed into a water bath for 24 h at room temperature to coagulate the dissolved cellulose. A drying process then followed, by taking out the frame with the samples from the water bath to dry for more than 48 h at room temperature.

Characterizations

Optical microscopy

Optic Microscopy (BH2-UMA, Olympus Corporation, Japan) was used to examine partially dissolved flax yarn morphology, alongside a CCD (Charge-coupled device) camera with a resolution of 1920×1200 for the capture of clear cross-sectional images. Each of the four processed samples were vertically embedded in epoxy resin after the resin and hardener (EpoxiCure 2, BUEHLER) were mixed at a 4:1 ratio, then the Teflon circular container was left at room temperature for 48 h. After that, a grinding and polishing process was applied to the yarns surface via a polishing machine (STRUERS ROTOPOL-11/ ROTOFORCE-1, Struers Ltd., UK) on the resin to produce a 1 to 2 cm thick sample prior to reflection analysis. To measure the ratio of the undissolved core (inner region) to the dissolved and coagulated fraction (outer region) of the processed yarns, 'ImageJ 1.52d' processing software was used to measure these two regions. Each partially dissolved composite yarn cross section was analysed 4 times for each condition of dissolution time and temperature (from the four samples wound on the frame, giving 16 individual measurements for each processing condition) and the average value and standard error were calculated. ImageJ 1.52d software was used to measure the area of the cross section from multiple directions on each sample (e.g., Fig. 3 in previous published (Albarakati et al. 2023)). All the partially dissolved composites showed the same structure of a central undissolved yarn surrounded by an outer ring of dissolved and coagulated cellulose. From these optical images, two specific parameters were used to measure the increase in the dissolved fraction and hence follow dissolution. First of these was the area fraction of the dissolved and subsequently coagulated material, called the coagulation fraction (CF) and then secondly the growth in the thickness of this outer coagulated layer. Both parameters have been examined at different processing temperatures and times.

The dissolution mechanism found in the ILs explored in this study, [C4mim][OAc] at 40 °C, 50 °C, 60 °C, and 70 °C, and [C2mim][Oct] at 80 °C, 85 °C, 90 °C and 100 °C were found to be very similar to that of the same flax yarn in the IL [C2mim][OAc], as detailed in the previous paper. The flax yarns are dissolved from outside and on coagulation in water the coagulated material forms an outer layer around the inner undissolved core, which we call the coagulated fraction (CF). Figure 2(a and b) shows the growth of this coagulated layer after various dissolution times and temperature for both ILs.

The growth of the thickness of the dissolved and coagulated region

A second set of observations were made from the optical images, by determining the difference in the diameters of the two regions. This growth of the thickness of the dissolved and coagulated region has enabled us to calculate the IL's diffusion, as the thickness growth was found to depend on the square root of the processing time.

The red double-arrow (T_H) indicates the average ring thickness of the flax samples, as shown in Fig. 3, and was calculated after repeating the two diameter measurements four times from multiple directions for each sample via Eq. 1:

$$T_H = \frac{DT - DC}{2} \quad (1)$$

Here DT is the outer ring diameter and DC the diameter of the undissolved yarn fraction.

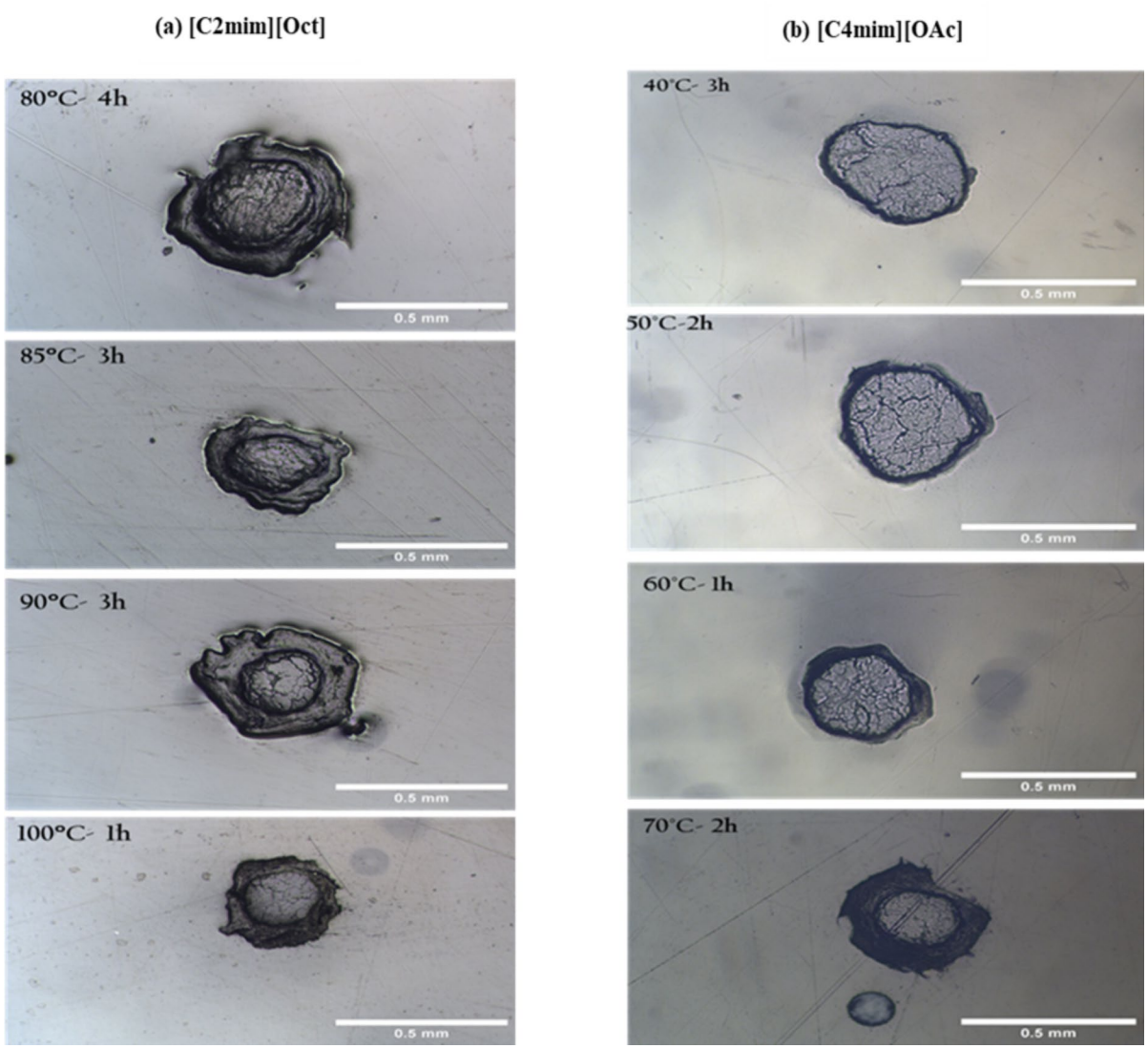

Fig. 2 Cross section images for partially dissolved flax yarns for both ILs showing the growth of the CF at various temperatures and times **a** [C2mim][Oct] and **b** [C4mim][OAc]. Scale length 0.5 mm

As there are four samples analysed for each time and temperature, this leads to a total of $4 \times 4 = 16$ measurements for each condition, giving an accurate calculation of the average thickness of the dissolved and coagulated layer.

Density

The densities of the three pure ILs [C4mim][OAc], [C2mim][Oct], and [C2mim][OAc] were measured at 20 °C using a graduated cylinder in MBraun Labmaster 130 glove box with a dry nitrogen atmosphere with a dewpoint level ranging between − 40 °C and − 70 °C to prevent water contamination in the IL samples. The IL used for the density measurements, were stored within this controlled environment ensuring minimum exposure to humidity.

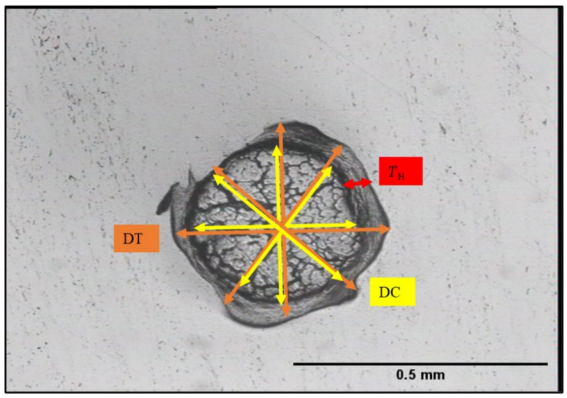

Fig. 3 Optical microscopy images of the cross section of the flax yarn, in which the total sample, the undissolved section, and the outer ring are indicated in orange (DT), yellow (DC) and red (T_H) double-arrow lines, respectively

Rheological measurements

The viscosity of the three different ionic liquids, as a function of shear rate, were studied using an Anton Paar 302 rheometer (Anton Paar GmbH, Graz, Austria). A plate- plate geometry with a diameter of 25 mm, and a gap size of 0.3 mm was used with temperature increasing from 30 °C to 100 °C. The Peltier hood was used to prevent water uptake by covering the edges of the plates from air. Newtonian behaviour was observed in all solvents at all temperatures, as evidenced by steady shear experiments conducted at shear rates ranging from 1 to 100 s^{-1}. Each sample was heated to the chosen temperature for one minute, and the measurements were conducted three times to determine an average viscosity value. The standard deviation in the measurements was found to be less than 10%.

^{1}H NMR (high- field) spectroscopy

The self-diffusion coefficient measurements of $[C2mim]^+$, $[C4mim]^+$, $[OAc]^-$ and $[Oct]^-$ ions were determined using a Bruker Avance II 400 MHz spectrometer. To measure the diffusion a Diff50 diffusion probe and a ^{1}H coil was utilized. We were able to achieve gradient strengths of up to 20 Tm^{-1}. The gradient field strength was calibrated by measuring the self-diffusion coefficient of water at a temperature of 20.0 ± 0.1 °C. This measurement involved using a heating element and dry airflow. Samples were given a minimum equilibration period of 10 min prior to each measurement. The pulsed-field gradient (PFG) technique was employed to measure self- diffusion coefficients, D. Gradient strength was varied stepwise, and D was obtained by applying the Stejskal-Tanner equation (Stejskal and Tanner 1965). The gradient pulse lengths, δ, ranged from 1 to 4 ms, whereas the diffusion times, Δ, varied from 10 to 100 ms. The uncertainty in the measurements was found to be 10%.

Results and discussions

Optical microscopy

Optical microscope cross sections were obtained and analysed for the processed samples using the partially dissolved composite yarns (for each set of four processed samples at the same processing time and temperature) after embedding in epoxy resin. The diameter for the raw flax yarn was calculated using the area determined via ImageJ software, 0.442 ± 0.002 mm^2. From these images, it can be clearly seen that the growth of the coagulation fraction is dependent on the dissolution time and temperature, so as the appearance of the dissolution process is similar to that of the [C2mim][OAc], time temperature superposition master curve can be explored and constructed.

Analysis of the dissolution of flax yarn in [C2mim][Oct] and [C4mim][OAc] using TTS approach

For the [C2mim][Oct], the dissolution process was started using a temperature of 50 ℃ within a specified time range (30 m, 1 h, 1.5 h, and 2 h), (as used for two acetate anion ILs [C4mim][OAc] and [C2mim][OAc]), but no observable signs of dissolution were detected even for 3 h processing time. Subsequently, the temperature was elevated to 60 ℃ at different dissolution times, but again no outer coagulation layer was observed, as illustrated in Fig. 4 (a), whereas the outer coagulation layer appeared at 60 ℃ for the [C4mim][OAc] as seen in Fig. 4 (b). In response to these outcomes, the temperature was further increased to 80 ℃, resulting in the formation of a coagulated fraction layer around the undissolved core

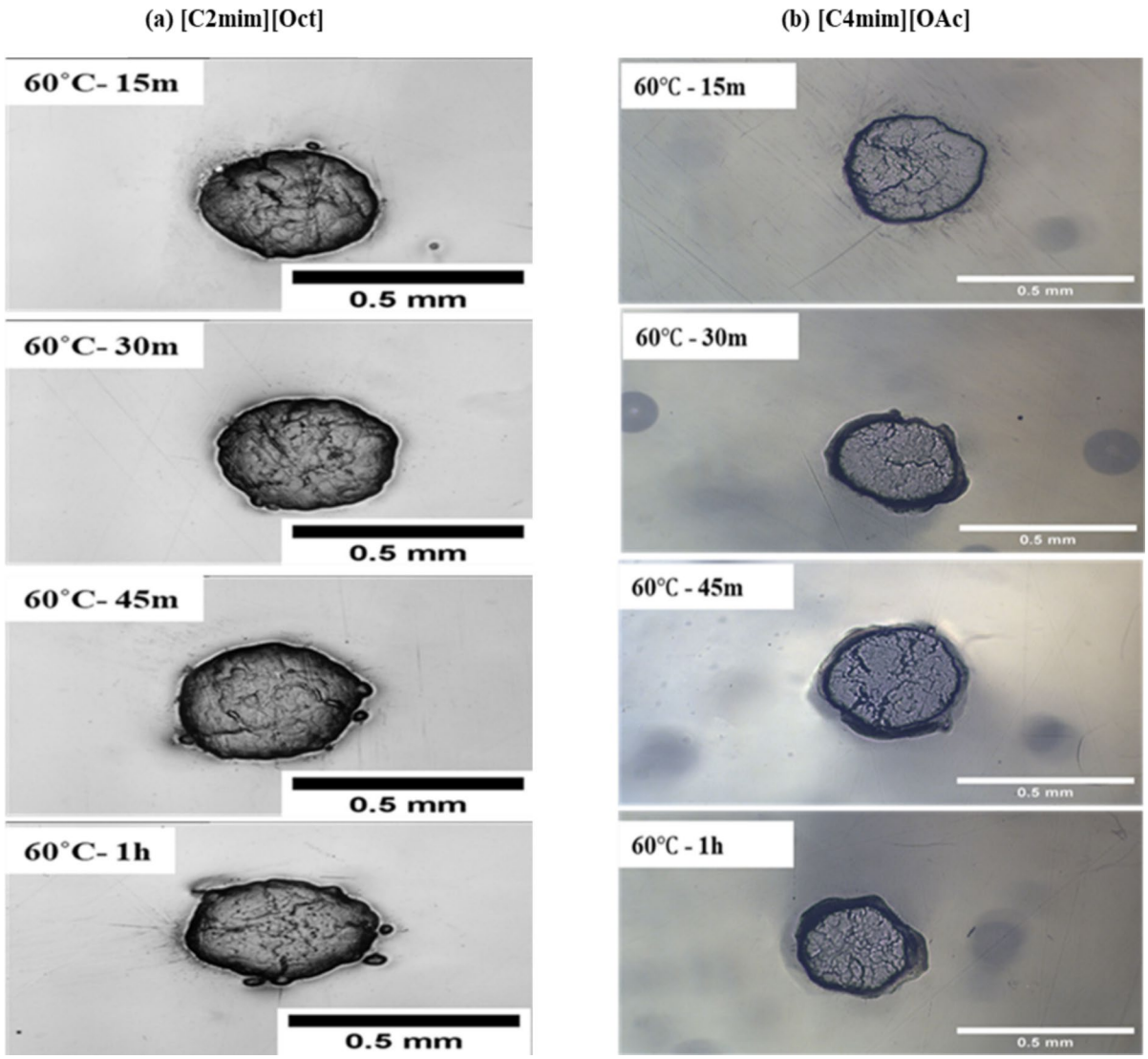

Fig. 4 Images showing cross sctions of processed fiber at 60 °C in arange of dissolution times 15 m, 30 m, 45 m and 1 h of the for both ILs. **a** no coagulation fraction seen for the [C2mim][Oct]. **b** shows the growth of CF as dissolution time increase for the [C4mim][OAc]

after 1 h processing time. The growth of the CF as a function of processing time and temperature and the steps used to determine an activation energy of dissolution via time temperature superposition is shown in Fig. 5. This is already an indication that the processing temperature has to be significantly higher for the IL [C2mim][Oct] compared to the two based on the acetate anion.

To analyse the growth of the fraction of the coagulated layer (called the coagulation fraction CF), and to create a master curve at a chosen reference temperature (here at 85 °C for the [C2mim][Oct] IL) the following steps were carried out. First, all the datasets were plotted together in one graph to show the growth of CF with the increase of time and temperature, as seen in Fig. 5(a). Next, the x-axis (time data) was converted to a natural logarithm time scale (ln (t)) to provide a visual guide for the shifting process. Then, the reference dataset of 85 °C was given a scaling factor $\alpha_{85} = 1$ and hence a natural logarithm value $\ln \alpha_{85} = 0$. Next, the datasets at the other processing temperatures of 80 °C, 90 °C, and

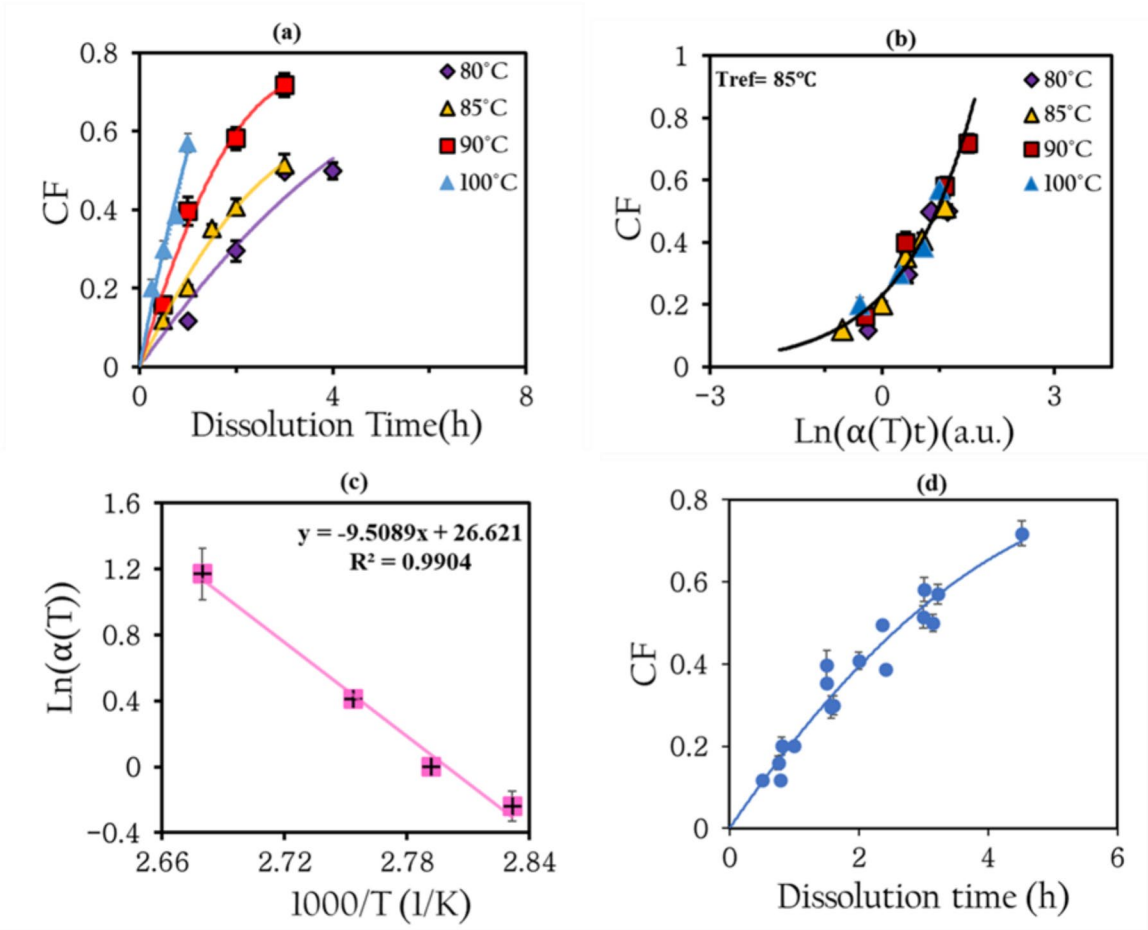

Fig. 5 **a** CF as function of all dissolution temperatures and times in [C2mim][Oct] at 85 °C, as reference temperature, polynomial fits used to guide the eye, and some error bars are smaller than data points. **b** Master curve of the coagulation fraction for all dissolution temperatures. Exponential fit used to guide eye, and some error bars smaller than data points. **c** Arrhenius plot presenting the relation between temperatures and shift factors, linear line fit to the data, and error bars included. **d** CF against the linear time shows the progress of the dissolution process for all temperatures and the line is polynomial with order two fit to the data

100 °C were shifting horizontally left or right by eye using a number equal to ln α_T to overlap with the reference data of 85 °C, creating a final master curve as shown in Fig. 5(b). The final data points were all fitted to the same exponential function and the coefficient of determination R^2 for the datasets was maximized by adjustment of the shift factors α_{80}, α_{90}, and α_{100}. A subsequent plot of the shift factors ln α_T with the inverse of the processing temperature, showed a linear relationship which indicates an Arrhenius behaviour, allowing an activation energy to be determined, see Fig. 5(c). The average activation energy required to dissolved flax yarn in the IL [C2mim][Oct] was found to be 79 ± 1 kJ/mol. Then we can finally plot the dissolution master curve against linear time which then describes how the dissolution rate is initially fast and then slows down as time progresses, as shown in Fig. 5(d). For the second new IL [C4mim][OAc], a similar procedure was used to analyse the growth of the coagulated fraction as a function of the processing time and temperature and the steps used to determine an activation energy of dissolution via time temperature superposition as described above is shown in Fig. S1. An average activation energy required to dissolved flax yarn in the IL [C4mim] [OAc] was found to be 67 ± 1 kJ/mol.

Investigating the growth of the thickness of the coagulated region with time and temperature for ILs [C2mim][OAc], [C2mim][Oct], and [C4mim][OAc]

Further analysis was conducted on the optical micrographs, using the same technique as described above for the time temperature superposition for the dissolution of flax yarn in the ILs, but this time measuring the difference in the diameters of the two regions and hence the thickness growth of the outer coagulated layer with processing temperature and time using Eq. 1. This was done for the two new ILs used for the dissolution studies reported above and also from a reanalysis of the results from the previous study using [C2mim][OAc]. The average thickness was then plotted first against linear time (t) and then against the root of the dissolution time ($\sqrt{t}$). The observed linear correlation between thickness and the square root of time is a strong indicator that the process in these systems follows Fick's law for diffusion see Eq. 2.

$$r \sim < r^2 >^{1/2} = (2D)^{1/2} * t^{1/2} \quad (2)$$

where r represents the root mean square distances that particles have moved from their original position, in diffusion time t, with diffusion D.

An Arrhenius equation was used to model the temperature dependence of the self-diffusion coefficient of the ions D.

$$\ln(D) = \ln\left(D_0\, e^{\frac{-E_A}{RT}}\right) = \ln(D_0) - \frac{E_A}{RT} \quad (3)$$

where $E_{A,D}$ is the activation energy of diffusion for the ions, T is the temperature, R is the gas constant, and D_0 is the pre-exponential factor.

For instance, the IL [C2mim][Oct] includes four processing temperatures, 80 °C, 85 °C, 90 °C and 100 °C; by using each temperature as a reference temperature, a master curve of the growth of the coagulation fraction at each temperature can be derived. The increase of the thickness of the coagulation layer with time was calculated at each reference temperature using Eq. 1. So, the results for increasing thickness were again plotted against the square root of time. Figure 6 shows typical data for [C2mim][Oct] at a reference temperature of 85 °C, and it is seen that the results fit well to a linear relationship between thickness and square root of time, indicating that the system is diffusion controlled/limited. Furthermore, the slope of each master curve can be used to calculate the diffusion coefficient by using Eq. 2. The slope of the line in the graph Fig. 6 can be related to the diffusion coefficient D of $(2.7 \pm 0.6)\times10^{-12} m^2/s$ at a reference temperature of 85 °C. The obtained diffusion coefficient are$(1.9 \pm 0.4)\times10^{-12} m^2/s$, $(4.2 \pm 0.8)\times10^{-12} m^2/s$ and $(7.9 \pm 1.4)\times10^{-12} m^2/s$ at 80 °C, 90 °C and 100 °C, respectively. The linear fit to the data with a high coefficient of determination $R^2 = 0.98$ indicates a very good correlation between the thickness and the square root of time. Interestingly, measuring the diffusion from the growth of the thickness of this outer coagulated layer by optical microscopy was explored for the first time in our group by (Alrefaei et al. 2023).

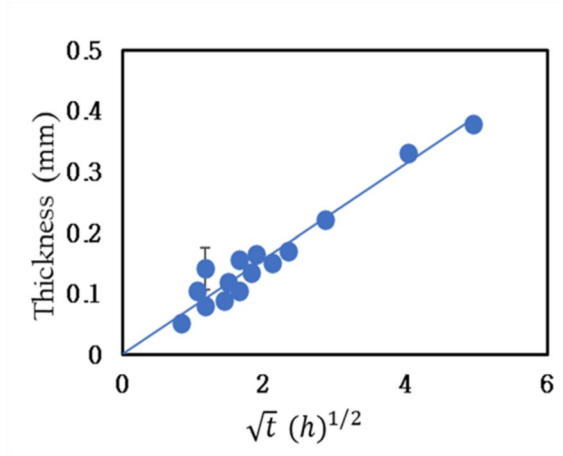

Fig. 6 Plot of the thickness vs. the square root of time in hours (h) for the IL [C2mim][Oct] at 85 °C, Error bars included

The same analysis was repeated for IL [C4mim][OAc] at temperatures of 40 °C, 50 °C, 60 °C and 70 °C and for IL [C2mim][OAc] at temperatures of 30 °C, 40 °C, 50 °C and 60 °C. They demonstrate that the thickness grows as a function of $\sqrt{t}$ obtained from the master curve for each temperature as a reference temperature. For the [C4mim][OAc], the diffusion values at each reference temperature 40 °C, 50 °C, 60 °C and 70 °C are $(3.3 \pm 0.3) \times 10^{-13} m^2/s$, $(8.5 \pm 1.0) \times 10^{-13}/s$, $(1.9 \pm 0.2) \times 10^{-12} m^2/s$, and $(3.3 \pm 0.3) \times 10^{-12} m^2/s$, respectively. The diffusion coefficients of the IL [C2mim][OAc] are $(6.2 \pm 1.1)\times 10^{-13} m^2/s$, $(1.2 \pm 0.2) \times 10^{-12} m^2/s$, $(3.4 \pm 0.6) \times 10^{-12} m^2/s$,

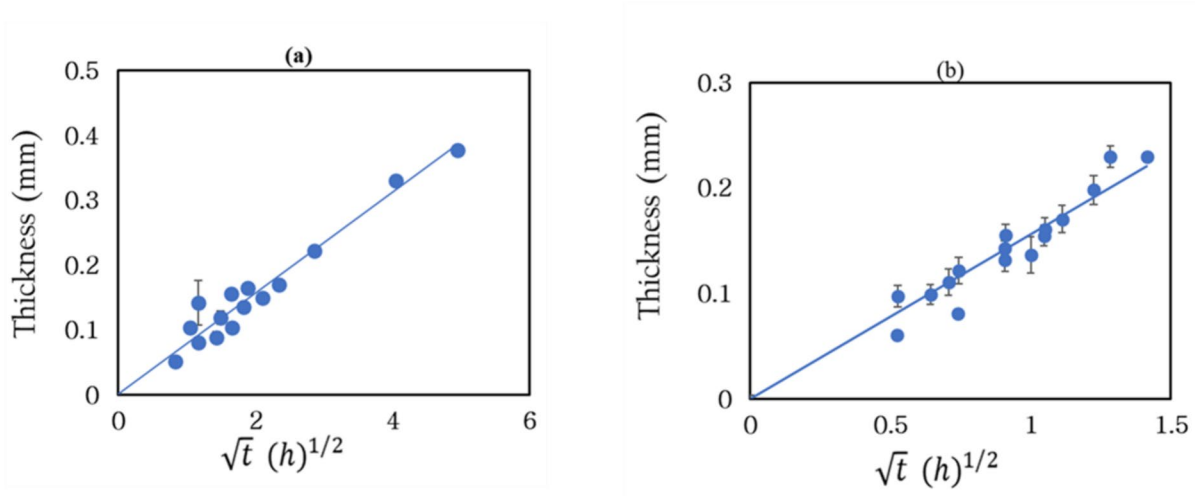

Fig. 7 Plots of the thickness vs. the square root of time in hours (h) for ILs at 50 °C, **a** [C4mim][OAc] and **b** [C2mim][OAc], and error bars included

Table 1 Activation energy values from two ways; coagulation fraction and thickness/diffusion for the three ILs

IL	Coagulation fraction E_A (kJ/mol)	Thickness/diffusion E_A (kJ/mol)
[C4mim][OAc]	67 ± 1	69 ± 5
[C2mim][Oct]	79 ± 1	77 ± 3
[C2mim][OAc]	64 ± 5	64 ± 6

and $(5.6 \pm 1.0) \times 10^{-12} m^2/s$ at reference temperature of 30 °C, 40 °C, 50 °C and 60 °C, respectively.

Figure 7(a and b) show again a typical result for a reference temperature of 50 °C for [C4mim][OAc] and [C2mim][OAc] and demonstrates that the thickness grows as a function of $\sqrt{t}$ for both systems. Our hypothesis is that because the coagulated region grows as the square root of the dissolution time, then the controlling factor for dissolution is the diffusion of the IL through the outer region which comprises dissolved cellulose and IL. Interestingly, the values of the diffusion activation energies calculated from Eq. 3 were found to be similar to those of the dissolution activation energies found earlier with values of 77 ± 3 kJ/mol, 69 ± 5 kJ/mol for [C2mim][Oct] and [C4mim][OAc], respectively. Also, the diffusion activation energy was similar to the dissolution activation energies that was found in the previous paper for the [C2mim][OAc] to be 64 ± 6 kJ/mol. A Table comparing the two ways to determine the activation energy, coagulation fraction and thickness/diffusion for the three ILs, is shown in Table 1.

Densities of pure ILs

The density measurements at 20 °C for the three pure ILs [C4mim][OAc], [C2mim][Oct], and [C2mim][OAc] are given in Table S1 with a list of density values for ILs obtained from our experimental measurements and values from literature. The density of the three ILs were determined as follow: first, using a glove box to minimise contamination, a small amount of the IL was carefully transferred into a graduated cylinder. Then, the mass of the IL was accurately measured using an analytical balance, while its volume was recorded from the graduated cylinder. After that, the density of the IL was calculated by dividing the measured mass by the recorded volume, yielding the density in units of g/cm^3. Next, the molar mass of the IL was obtained from its chemical formula, and the molar volume was determined by dividing the molar mass by the calculated density. This step provides the molar volume of the IL in cubic metres (m^3) in order to determine the size of each

IL. Determining the molar volume is essential for estimating the size of each IL, as it directly influences the accuracy of the hydrodynamic radius evaluation. This will be further analyzed and discussed in a later section.

Rheology measurements of pure ILs

The average value of viscosity for each IL was calculated from the Newtonian shear rate for each temperature and the measurements were repeated three times to calculate an average value of viscosity, and the standard deviation in the measurements was calculated. The viscosities η for ILs [C2mim][OAc], [C4mim][OAc] and [C2mim][Oct] as a function of temperatures ranging from 30 ˚C to 80 ˚C were measured. Figure S2 (a and b) shows viscosity as a function of shear rate for pure ILs [C4mim][OAc] and [C2mim][OAct] calculated from the Newtonian shear rate for each temperature, averaged over three measurements. Each IL presents a decreasing viscosity as temperature increases, with [C2mim][Oct] having a higher viscosity than [C2mim][OAc] and [C4mim][AOc] across the temperature range studied. This is due to the longer chain of the octanoate anion, and the higher molecular weight make the molecules moves slower and making fewer attempts to overcome the barriers, leading to an increase in the viscosity at all temperature. While, [C4mim][OAc] has a lower molecular weight, its molecules move faster, making more attempts to overcome barriers, which lowers its viscosity at all temperature. Figure S2 (c) presents a comparison of the viscosity of the three ILs [C2mim][OAc], [C4mim][OAc] and [C2mim][Oct] as a function of shear rate at a chosen temperature of 50 °C. The IL [C2mim][OAc] showed a noticeable decrease in viscosity compared to the two ILs [C4mim][OAc], and [C2mim][Oct], however, the IL [C2mim][Oct] has a higher viscosity compared to other two and this might be due to the anion's longer chain (Oct). The length and also the structure of both cation and anion significantly affect viscosity as expected. The activation energies were found by using the slope of Arrhenius plots for the viscosity data, as seen in Fig. S2 (d). The plots of ln (η) against inverse temperature are linear in the range of temperatures studied. The viscosity as a function of shear rate of the pure [C2mim][OAc] is in good agreement with the published data in (Green et al. 2017; Quijada-Maldonado et al. 2012; Ries et al. 2014; Victoria et al. 2022), as seen in the Fig. S3.

Seki et al. (2010) measured the viscosity of various room-temperature ionic liquids and analysed how different cations and anions affect these properties. They found that the viscosity of both cationic and anionic were significantly influenced by their molecular geometry (shape) rather than the molecular weight (Seki et al. 2010). In addition, the study by Green et al. (2017) discusses how the presence of the acetate anion [OAc] in both [C2mim] and [C4mim] results in more powerful ionic interactions compared to the octanoate ([Oct]) anion in [C2mim][Oct], this difference in interactions leads to various viscosity attributes at different shear rates. Specifically, the acetate anion forms small, stable aggregates that are less sensitive to flow and temperature changes, whereas the octanoate anion forms larger, less stable aggregates that decrease in size with increased flow and temperature (Green et al. 2017). Yadav et al. (2018) discussed the densities and dynamic viscosities of ionic liquids with different cations and anions. They observed that the anion type significantly controls the density and viscosity (Yadav et al. 2018). The molecular weight and therefore the size of IL is expected to increase the viscosity of the IL. An extensive study by Budtova and Navard (2015) found that the viscosity of cellulose solutions increases with its molecular weight due to the higher molecular weights suggest longer polymer chains, which entangle more easily and increase flow resistance (Budtova and Navard 2015).

These findings indicate that [C4mim][OAc] needs a higher amount of energy to overcome the molecular interactions for flow in comparison to [C2mim][OAc], and [C2mim][Oct]. These differences can be related to the higher viscosity resulting from the longer cation chain [C4mim]. While the difference between the common cation, [C2mim], and the differences in anions (Oct) and (OAc), their interactions with the [C2mim] cation led to it exhibiting higher viscosity energy barriers for viscous flow of (Oct) due to the longer anion chain. It is also interesting to note that the viscosity activation energies of the pure ILs are significantly lower than that found in the dissolution experiments. This enhances our hypothesis that the diffusion coefficients determined from the growth of the coagulated regions refers to the diffusion of the

ILs in an IL/cellulose solution, not just the diffusion of the pure ILs themselves.

^{1}H NMR of pure ILs

The high field ^{1}H NMR spectrum (400 MH_Z) for the three pure ILs are shown in Fig. S4. It can be observed how the self-diffusion coefficient of the anion and cation of pure ILs changes with temperature (30 °C, 40 °C, 50 °C and 60 °C) using ^{1}H NMR spectroscopy. This method allows the molecular mobility of the pure ionic liquid to be studied, offering insights into its dynamic behaviour. Importantly each ion (cation and anion) can be studied separately. The spectrum with full peak assignments, which correspond to the various proton environments (H1– H7), (H1- H9), and (1H-10H) of [C2mim][OAc], [C4mim][OAc], and [C2mim][Oct], respectively, were shown above Fig. 1. In our work, we used the proton resonance (peak 5) as a reference point to determine the chemical shift of all the other resonances by measuring their distances from this peak. Previous studies have demonstrated that the chemical shift position of the methyl group (peak 5) is least affected (Ries et al. 2014; Zhang et al. 2010; Zhao et al. 2008) by external factors. Both the anion and cation for each IL show an increase in intensity as temperature increase suggesting that molecular mobility for both ions also increases with temperature. Higher temperatures lead to lower viscosity and higher diffusion rates (Zhang et al. 2015).

The diffusion data could be used to calculate the activation energy for self-diffusion of the cation and anion for each IL, as seen in Fig. 8(a) for the cation and (b) for the anion. Arrhenius plots Eq. 3, which graph the natural logarithm of diffusion coefficients versus the inverse of temperature (in kelvin), provides the activation energies, indicating the sensitivity of diffusion to temperature changes. ILs show a linear trend within the temperature range studied. The activation energies obtained from the Arrhenius plots are given in Table 2 for both ions. Table 2 represents

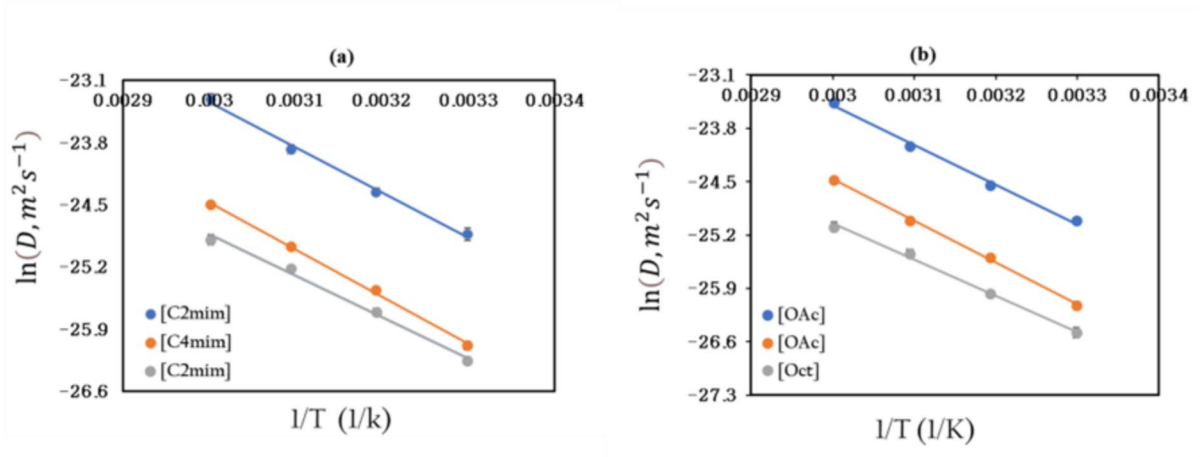

Fig. 8 Natural logarithim of self-diffusion coefficients for the three ILs as a function of the inverse temperature. **a** The cation and **b** The anion. Linear fits show for the lines and the uncertainty in D is approximately the size of point of 10%. The blue, red, and grey lines are for [C2mim][OAc], [C4mim][OAc], and [C2mim][Oct], respectively

Table 2 The activation energies of the NMR diffusion of cation and anion for the three ILs, along with the corresponding activation energies derived from viscosity measurements

ILs	[C2mim][OAc]	[C4mim][OAc]	[C2mim][Oct]
NMR D. cation E_a (kJ/mol)	42 ± 2	44 ± 1	38 ± 2
NMR D. anion E_a (kJ/mol)	43 ± 2	45 ± 1	39 ± 3
Viscosity $(E_{a,\eta})$(kJ/mol)	37 ± 1	46 ± 2	40 ± 1

the activation energy values of the three ILs were obtained from NMR diffusion measurement, which is very close to the corresponding activation energies derived from viscosity measurements. so ILs follow a Stokes–Einstein relationship (Lovell et al. 2010). Since the imidazolium anion is smaller than cation and therefore the diffusion of anion is expected to be faster than cation, but experimentally this is not the case. This unexpected slower diffusion of the anion is related to the rich aggregation in anion compered to cation, as suggested in (Hou et al. 2011). Ion diffusivities are influenced by ions' size, shape, and intensity of interactions (Zhao et al. 2008).

Stokes–Einstein- analysis and radius of ions

The linear correlation in the experimental data of Fig. 9 demonstrates that the Stokes–Einstein Eq. 4 provides a suitable description of the relationship between the self- diffusion coefficient D, and the ratio of temperature to the zero-shear rate viscosity T/η for the systems of [C2mim][OAc], [C4mim][OAc], and [C2mim][Oct], as given in Fig. 9. The gradients from the Stokes–Einstein fitting are used to calculate the values of hydrodynamic radius $R_{h,_i}$.

$$D = \frac{k_B T}{6f\pi\eta R_{h,i}} \tag{4}$$

where k_B is the Boltzmann constant, $R_{h,i}$ is the hydrodynamic radius. The value of "f" is a pre- factor (Antony et al. 2005).

Various studies have shown that a pre-factor of $f = 2/3$ is suitable for a variety of molecular liquids (McLaughlin 1959; Tokuda et al. 2004), so this value has been applied to the Stokes − Einstein analysis in this study due to the diffusing particles being of a similar size to the surrounding diffusing molecules. Experimentally, the values of the $R_{h,_i}$ are 2.19 Å and 2.57 Å, for the cation and anion of [C2mim][OAc], respectively. The values of the $R_{h,_i}$ are 2.47 Å and 2.54 Å, for the cation and anion of [C4mim][OAc], respectively. For the radius of the cation and anion at [C_2mim][Oct] are 2.75 Å and 3.40 Å, respectively. The average values of $R_{h,_i}$ for the ILs [C2mim][OAc], [C4mim][OAc] and [C2mim][Oct] are 2.28 Å, 2.51 Å and 3.07 Å, respectively. These results acquired using the slopes of each ion from the SE approach which

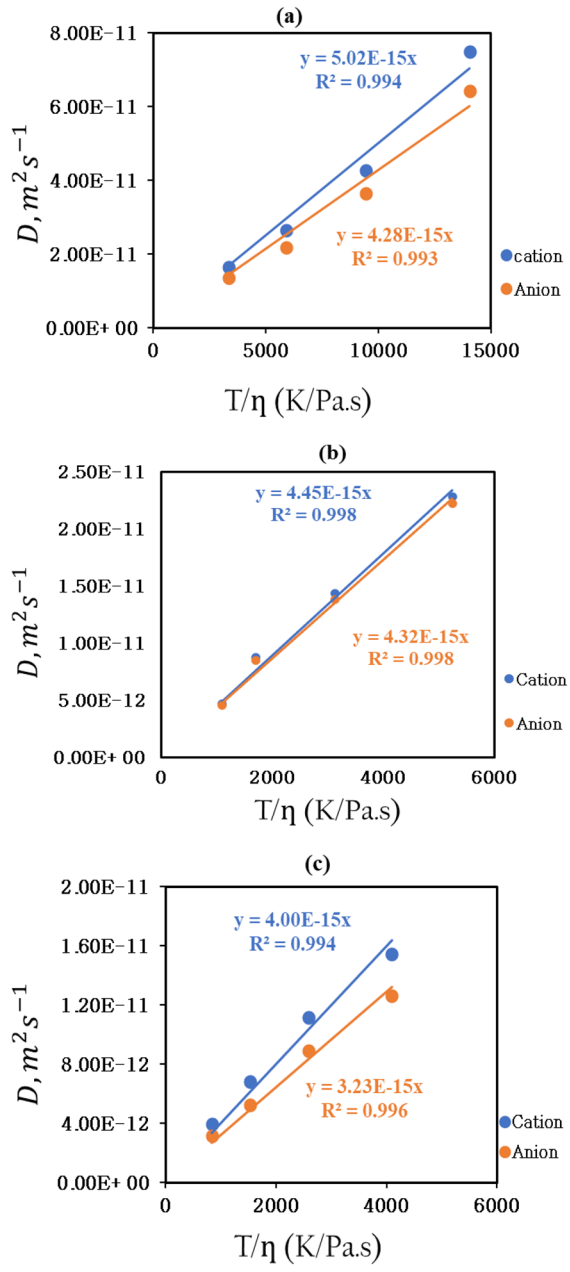

Fig. 9 Correlation between D and T/η for the cation and anion in the ILs. **a** [C2mim][OAc]. **b** [C4mim][OAc], and **c** [C2mim][Oct]. The solid lines are fits to the Stokes–Einstein equation calculated from Eq. 4

referred as Stokes–Einstein values (SE) and are determined from Fig. 9.

The hydrodynamic radius, $R_{h,i}$, can be related to the molar mass of the liquids by the approximation:

$$R_{h,i} = \frac{1}{2}\left(\frac{M}{\rho N_A}\right)^{1/3} \quad (5)$$

where N_A is the Avogadro number; M the molar mass of the liquid; and ρ the density.

To calculate the hydrodynamic radius $R_{h,i}$ theoretically by measuring the density refer to Eq. 5, the values of R_{h_i} for the IL [C2mim][OAc] is 3.13 Å. The effective values of R_{h_i} were found to be 2.72 Å and 2.20 Å for the [C2mim] and [OAc], respectively, which are close to previously published values of 2.74 Å and 2.24 Å (Hall et al. 2012). The values of R_{h_i} for the ILs [C4mim][OAc] is 3.41 Å, and the effective values of R_{h_i} were found to be 3.03 Å and 2.28 Å for the [C_4mim] and [OAc], respectively, which are close to previously published values of 3.01 Å and 2.26 Å (Lefroy et al. 2021). The values of R_{h_i} for the IL [C2mim][Oct] is 3.65 Å, and for the radius of the [C2mim] and [Oct] are 2.77 Å and 3.01 Å, respectively, which are close to previously published values of 2.86 Å and 3.11 Å (Green et al. 2017).

Investigating the dissolution speed and mechanisms of the three ILs: [C2mim][OAc] [C4mim][OAc] and [C2mim][Oct] at 60 °C

To do a comparison between the three ILs investigated, it is necessary to compare them all at the same reference temperature. The chosen temperature was 60 °C as the two acetate anion ILs ([C2mim][OAc] [C4mim][OAc]) dissolved at a significant rate at this temperature. However (as shown in Fig. 4a) the Octanoate anion in the IL [C2mim][Oct], did not dissolve significantly at this temperature in a few hours. As this temperature was below the measured temperature range for [C2mim][Oct], data had to be synthesised at 60 °C using TTS. First, using the Arrhenius equation again, but this time create the data at 60 °C, by adjusting the data to reflect a temperature change from 80 °C to 60 °C, so the linear equation at 80 °C is $Y = -9.5088\ x + 26.935$, where Y is ln(α) and x is 1000/T. To compute the ln(α) for 60 °C by determine 1000/T for this temperature, which is 3.001651. Substituting this value into the equation is approximately -1.6071. By determining the difference between the calculated ln(α) at 60 °C and the actual ln(α) at 80 °C, this difference used to adjust the data by shifting the values from 80 °C to 60 °C. Now, these adjusted values form a new master curve at 60 °C, which used to compare with other ILs.

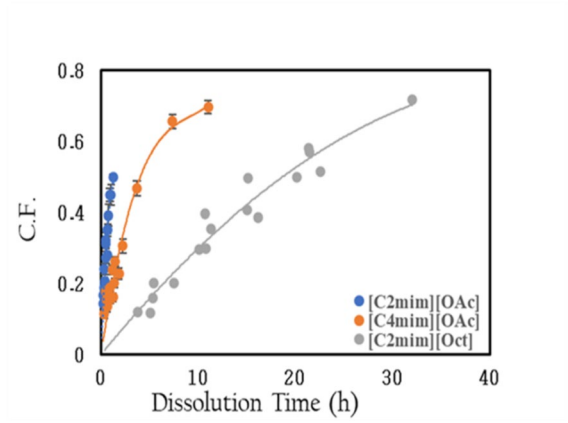

Fig. 10 Master curves for the three ILs for the coagulation fraction (C.F.) as a function of dissolution time (h) at temperature of 60 °C

Figure 10 shows a comparison of the growth of the coagulation fraction as function of dissolution time for all three ILs at a reference temperature of 60 °C. The differences between the three ionic liquids based on the information provided in the plot indicate that the IL[C2mim][OAc] has the fastest dissolution rate among the three, followed by the other acetate anion IL [C4mim][OAc]. The slowest dissolving rate is exhibited by [C2mim][Oct], as demonstrated by its CF curve. These differences could be due to the length of the alkyl chain in the cation or the nature of the anion in the ionic liquids or the molecular weight of the ILs. Huddleston et al. (2001) carried out an investigation of ILs that contained [$C_n$mim]$^+$ cations and a variety of anions in order to determine the effects of altering the length of the cation chain (Huddleston et al. 2001). They compared the alkyl side-chain lengths between octyl ($n = 8$) and methyl ($n = 1$), so an increase in the chain length was observed to result in a uniform increase in viscosity, a decrease in melting point, and a reduction in density for the same anion. Moreover, longer chains typically resulted in lower solubility, which seems to be demonstrated by the difference between [C2mim] and [C4mim]. This is due to the hydrophobic interactions increased throughout longer chains, leading to a more ordered structure (Freire et al. 2012; Wang and Voth 2006). Moreover, the anion difference between [OAc]

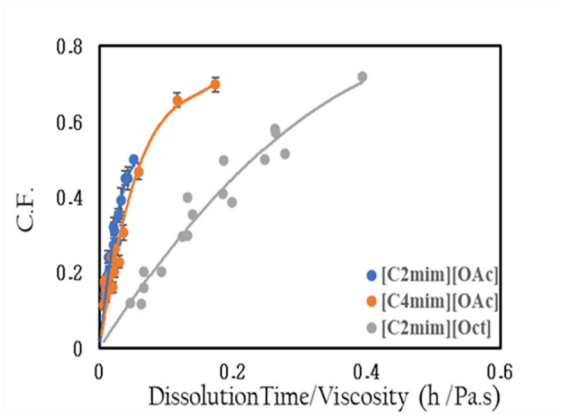

Fig. 11 Master curves for the three ILs for the coagulation fraction (C.F.) as a function of dissolution time /Viscosity (h/Pa.s) at temperature of 60 °C

(acetate) and [Oct] (octanoate) also seems to play a significant role in the dissolution characteristics.

One factor that could be important in affecting the dissolution speed is the pure IL viscosity. To study this effect, the results from Fig. 10 were plotted with the x-axis now normalised by the measured viscosities. The datasets aim to eliminate the direct impact of viscosity on the dissolving rate by dividing the dissolution time by viscosity. This means that the time scales are determined by viscosity, so large time scales will give large viscosity, so we normalise the times by using viscosity, as seen in Fig. 11. It is clearly seen that the two-acetate based ILs, [C2mim][OAc] and [C4mim][OAc] when the viscosity is taken into account, nearly overlap. In going from the [C2mim] to [C4mim] the cation is larger which slows diffusion and raises viscosity, but it has not significantly changed any other dissolution factor. When the anion is changed to octanoate then the data no longer overlaps with the acetate results, even when taking into account the change of viscosity. This hints at the more important role that the anion plays in the dissolution process.

In the next comparison (Fig. 12a and b) the dissolution time x-axis has been normalised by the self-diffusion coefficient of the cations and anions measured from NMR. Here we multiply the time by the diffusion coefficient to take into account the greater mobility and its effects on dissolution timescales. A large D would suggest a short dissolution time. Figure 12 shows that with this normalisation the results are very similar to the viscosity normalisation of Fig. 11. [C2mim][OAc] and [C4mim][OAc] have a similar relationship between the growth of the coagulation fraction and normalised time (using either the cation or anion diffusion coefficients) and as for Fig. 11, [C2mim][Oct] results shows a slower overall dissolution process even when normalised.

Using either solution viscosity or NMR IL ion self-diffusion, the results with the same anion collapse to

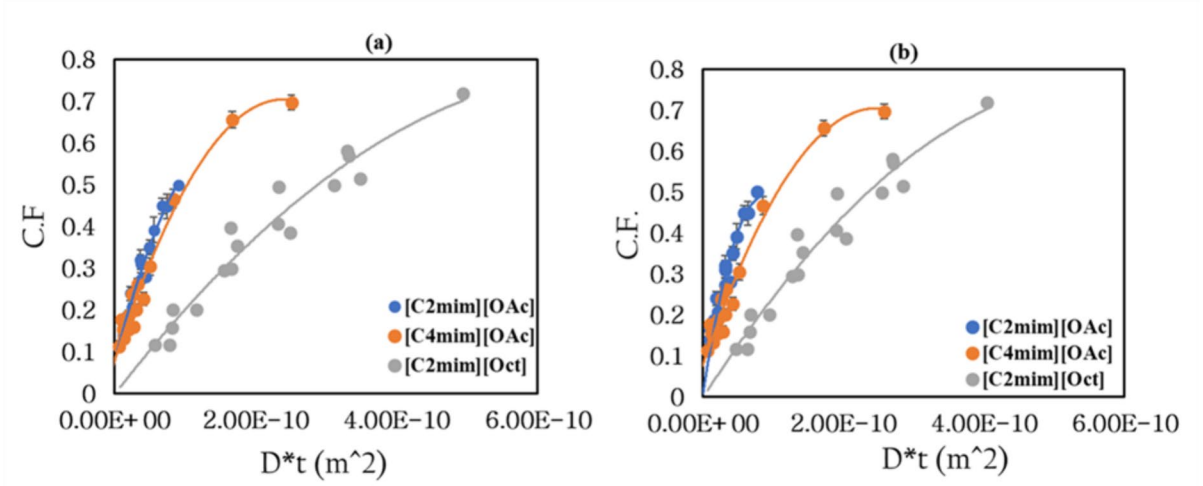

Fig. 12 Master curves for the three ILs for the coagulation fraction (C.F.) as a function of the D*t measured from NMR at temperature of 60 °C of the (**a**) cations and **b** anions

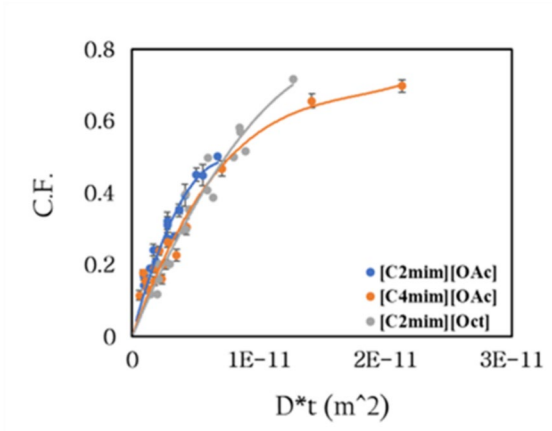

Fig. 13 Master curve representing the results of the three ILs at temperature of 60 °C for the coagulation fraction (C.F.) as function of the D*t. from thickness measurements

a similar dissolution curve, but the different anion is still slower. For the final normalisation, the dissolution time is normalised by the diffusion coefficients calculated directly from the growth of the thickness of the coagulated region and these results are shown in Fig. 13. It is seen that normalising the dissolution time by this factor, that all data collapses onto a set of overlapping curves. Our hypothesis is therefore that the dissolution of the flax yarn is controlled by the diffusion of each IL through a saturated cellulose solution that surrounds each flax yarn as the dissolution progresses, such that when you take into account the additional slowing down of the ions due to the presence of cellulose, a master curve can be obtained.

A measure of the relative speed of dissolution in the three ILs can be obtained by shifting the generated master curves at 60 °C to make them overlap. Figure 14 below shows the datasets of the three ILs [C2mim][OAc], [C4mim][OAc] and [C2mim][Oct] in order to calculate the relative dissolution rates between systems. The procedure of forming these master curves was described in the TTS method shown in Fig. 5 and in Fig. S1, and the TTS Fig. 6 in our previous paper, so by choosing the data of [C2mim][OAc] as reference data, then shifting all the data again for these systems with now each master curve itself shifted separately in natural logarithmic time to overlap with the master curve of [C2mim][OAc] to create a master-master curve. So, for example, to overlap the data of [C4mim][OAc] with the master curve of the data of [C2mim][OAc], needed a scaling factor α of 0.25, determined from the shift factor ln(α). Hence, the dissolution rate is 4 times slower for this system. So, the shift factors of each IL that used to create the master-master curve can use to measure the relative dissolution speed of each IL directly. The obtained shift factor ln(α) and relative dissolution rates are summarised in Table S2.

By plotting the relationship between the relative dissolution speed of each IL and their size to determine the relative dissolution speed between systems. The effective size of each IL was measured by (Eq. 5), utilising the molar mass as the input parameter, as

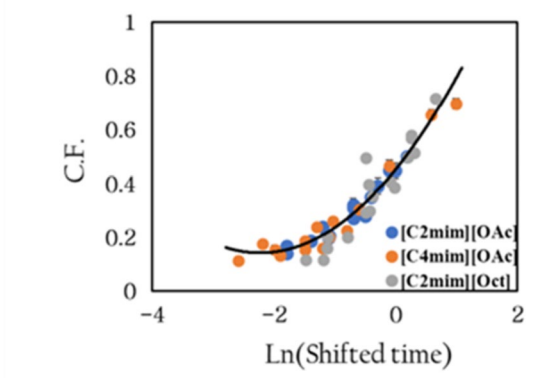

Fig. 14 Master curve for the three ILs for the coagulation fraction (C.F.) as a function of Ln(shifted time) to calculate the relative dissolution rate between systems

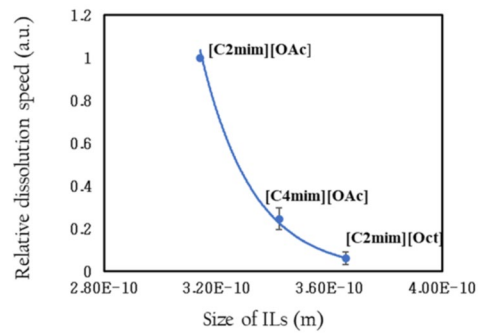

Fig. 15 Master-master curve shows all the results of ILs to calculate the relative dissolution rate between systems. The exponential fit of the relationship is such that as the size of the ILs increases, the relative dissolution speed decreases rapidly

detailed in the density section. The plotted line suggests that as the size of the ILs increases, the relative dissolution speed decreases rapidly, see Fig. 15. This implies that the differences in hydrodynamic radii of (ILs) have an important impact on the ability to dissolve cellulose. The IL [C2mim][OAc] shows a smaller ion, which might have a greater ability to penetrate the cellulose structure, therefore disrupting the hydrogen bonds between cellulose chains compared to other ILs. The IL [C2mim][Oct] might be less efficient in breaking down cellulose due to their larger size, which can prevent their ability to penetrate the tightly packed cellulose network. The dotted line of the graph shows a clear decay trend, indicating dissolution speed is inversely related to the size of the ILs. Broadly speaking, the [C2mim][OAc] is 5 times faster than [C4mim][OAc], and 10 times than [C2mim][Oct].

Conclusion

In this paper, we have investigated the dissolution behaviour of flax yarns in the imidazolium- based ILs [C4mim][OAc] and [C2mim][Oct] in both macroscopic and microscopic properties over a range of time and temperatures. These results are compared and combined with previous published work on (1-ethyl-3-methylimidazolium acetate) ($[C2mim]^+[OAc]^-$) in the same flax yarns. This work reveals the role of cation and anion structure on the dynamics of cellulosic yarn dissolution. The dissolution process involved submerging the yarns in the ILs for a range of temperatures and times, followed by coagulation in water. The coagulated material formed as an outer ring that surrounded the central undissolved yarn. Optical microscopy was used to follow this growth revealing an Arrhenius behaviour, enabling the determination of the dissolution activation energy. The dissolution activation energies of the ILs [C4mim][OAc] and [C2mim] [Oct] were found to be 67 ± 1 kJ/mol and 79 ± 1 kJ/mol, respectively. The growth of the thickness of the outer coagulated later was measured also for each processed yarn as one of important key to calculate the diffusion coefficients. The dataset of thickness as a function of the square root of time showed a linear relationship, this is indicative that diffusion controlled the dissolution process. The calculated diffusion activation energies from the growth of thickness of ILs [C2mim][Oct], [C4mim][OAc] and [C2mim[OAc] were found to be 77 ± 3 kJ/mol, 69 ± 5 kJ/mol and 64 ± 5 kJ/mol, respectively.

The viscosities were measured for all the three ILs [C4mim][OAc], [C2mim][Oct] and [C2mim][OAc], and as expected decreased when temperature is increased. The IL [C2mim][OAc] shows a noticeably lower viscosity compared to the two ILs [C4mim][OAc] and [C2mim][Oct], with [C2mim][Oct] having the highest viscosity. The viscosity activation energy for [C4mim][OAc], [C2mim][Oct] and [C2mim][OAc] were found to be 46 ± 2 kJ/mol, 40 ± 1 kJ/mol and 37 ± 1, respectively.

NMR self-diffusion coefficient for each component $[C4mim]^+$,$[OAc]^-$,$[C2mim]^+$ and $[Oct]^-$ were measured. It was found that larger cations $[C4mim]^+$ and $[C2mim]^+$ diffuses faster than their anionic counterparts $[OAc]^-$ and $[Oct]^-$ in the ILs. The activation energies value obtained from NMR diffusion measurement are in agreement with that of viscosity for the three ILs, so the ILs follow a Stokes–Einstein relationship. Finally, normalising the dissolution results by the diffusion from the thickness analysis collapses all the dissolution data onto one master curve. This suggest that it is the diffusion of each IL through a swollen solution of cellulose that is the controlling factor, rather than the self-diffusion/viscosity of the pure IL. The key conclusion is therefore that the rate of dissolution of the flax yarns (in all three ILs) is controlled and limited by the diffusion of each IL through a region of swollen cellulose/IL around each yarn as it dissolves. This is an important result for controlling the fraction of coagulated material (and hence mechanical properties) in, for example, all-cellulose composites.

Acknowledgments The authors are greatly thankful to Dr. Daniel Baker in Soft Matter Group from School of Physics and Astronomy for experiment training and help, as well as my colleagues in the office (1.12) for a great discussion to make this research possible. The authors are also grateful to Umm Al-Qura University for funding this work.

Author contributions Fatimah A. Albarakati: Methodology, Investigation, Formal analysis, Writing- original draft. Micheal E. Ries: Supervision, Conceptualization, Methodology, Data curation, Writing- review & editing, Project administration. Peter J. Hine: Supervision, Conceptualization, Methodology, Data curation, Writing – review & editing, Project administration.

Funding This research was funded through a studentship from Umm Al-Qura University, Makkah, Saudi Arabia.

Data availability The datasets generated during and/or analysed in the current study are available from the corresponding author on request. The data associated with this paper are openly available from the University of Leeds Data Repository, https://doi.org/10.5518/1663

Declarations

Conflict of interests The authors declare that they have no conflict of interest.

Consent to participate All authors consent to participating in this work.

Consent for publication All authors have given consent for this publication, which includes text, photographs, figures and details within the text to be published in the journal "Cellulose".

References

Albarakati FA, Hine PJ, Ries ME (2023) Effect of water on the dissolution of flax fiber bundles in the ionic liquid 1-ethyl-3-methylimidazolium acetate. Cellulose 30(12):7619–7632

Alghamdi AS, Hine PJ, Ries ME (2024) Time-temperature superposition of the dissolution of Wool yarns in the ionic liquid 1-ethyl-3-methylimidazolium acetate. Materials 17(1):244

Alrefaei NS, Hine PJ, Ries ME (2023) Dissolution of hemp yarns by 1-ethyl-3-methylimidazolium acetate studied with time-temperature superposition. Cellulose 30(16):10039–10055

Antony JH, Dölle A, Mertens D, Wasserscheid P, Carper WR, Wahlbeck PG (2005) 13C NMR relaxation rates in the ionic liquid 1-methyl-3-nonylimidazolium hexafluorophosphate. J Phys Chem A 109(30):6676–6682

Bochek A (2003) Effect of hydrogen bonding on cellulose solubility in aqueous and nonaqueous solvents. Russ J Appl Chem 76(11):1711–1719

Bonifacio A, Bonetti L, Piantanida E, De Nardo L (2023) Plasticizer design strategies enabling advanced applications of cellulose acetate. Eur Polym J. https://doi.org/10.1016/j.eurpolymj.2023.112360

Budtova T, Navard P (2015) Viscosity-temperature dependence and activation energy of cellulose solutions. Nord Pulp Pap Res J 30(01):99–104

Bylin S, Olsson C, Westman G, Theliander H (2014) Solvation behavior of cellulose and xylan in the MIM/EMIMAc ionic liquid solvent system: parameters for small-scale solvation. BioResour 9(1):1038–1054

Chen F, Sawada D, Hummel M, Sixta H, Budtova T (2020) Swelling and dissolution kinetics of natural and man-made cellulose fibers in solvent power tuned ionic liquid. Cellulose 27(13):7399–7415

Cho HM, Gross AS, Chu J-W (2011) Dissecting force interactions in cellulose deconstruction reveals the required solvent versatility for overcoming biomass recalcitrance. J Am Chem Soc 133(35):14033–14041

El Seoud OA, Bioni TA, Dignani MT (2021) Understanding cellulose dissolution in ionic liquid-dimethyl sulfoxide binary mixtures: quantification of the relative importance of hydrogen bonding and hydrophobic interactions. J Mol Liq 322:114848

Erdmenger T, Haensch C, Hoogenboom R, Schubert US (2007) Homogeneous tritylation of cellulose in 1-butyl-3-methylimidazolium chloride. Macromol Biosci 7(4):440–445

Feng L, Chen Z-l (2008) Research progress on dissolution and functional modification of cellulose in ionic liquids. J Mol Liq 142(1–3):1–5

Fernandes AM, Rocha MA, Freire MG, Marrucho IM, Coutinho JA, Santos LM (2011) Evaluation of cation–anion interaction strength in ionic liquids. J Phys Chem B 115(14):4033–4041

Freire MG, Neves CM, Canongia Lopes JN, Marrucho IM, Coutinho JoA, Rebelo LPN (2012) Impact of self-aggregation on the formation of ionic-liquid-based aqueous biphasic systems. J Phys Chem B 116(26):7660–7668

Green SM, Ries ME, Moffat J, Budtova T (2017) NMR and rheological study of anion size influence on the properties of two imidazolium-based ionic liquids. Sci Rep 7(1):1–12

Gupta KM, Jiang J (2015) Cellulose dissolution and regeneration in ionic liquids: a computational perspective. Chem Eng Sci 121:180–189

Hall CA, Le KA, Rudaz C, Radhi A, Lovell CS, Damion RA, Budtova T, Ries ME (2012) Macroscopic and microscopic study of 1-ethyl-3-methyl-imidazolium acetate–water mixtures. J Phys Chem B 116(42):12810–12818

Hawkins JE, Liang Y, Ries ME, Hine PJ (2021) Time temperature superposition of the dissolution of cellulose fibres by the ionic liquid 1-ethyl-3-methylimidazolium acetate with cosolvent dimethyl sulfoxide. Carbohydr Polym Technol Appl 2:100021

Hou J, Zhang Z, Madsen LA (2011) Cation/anion associations in ionic liquids modulated by hydration and ionic medium. J Phys Chem B 115(16):4576–4582

Hua L, Li R-Z, Mu R-H, Hou H-Y, Ma T-T (2024) Molecular dynamics study on effects of the synergistic effect of anions and cations on the dissolution of cellulose in ionic liquids. J Mol Liq 415:126348

Huddleston JG, Visser AE, Reichert WM, Willauer HD, Broker GA, Rogers RD (2001) Characterization and comparison of hydrophilic and hydrophobic room temperature ionic liquids incorporating the imidazolium cation. Green Chem 3(4):156–164

Ju Z, Yu Y, Feng S, Lei T, Zheng M, Ding L, Yu M (2022) Theoretical mechanism on the cellulose regeneration from a cellulose/EmimOAc mixture in anti-solvents. Materials 15(3):1158

Klähn M, Lim GS, Seduraman A, Wu P (2011) On the different roles of anions and cations in the solvation of enzymes in ionic liquids. Phys Chem Chem Phys 13(4):1649–1662

Lefroy KS, Murray BS, Ries ME (2021) Rheological and NMR studies of cellulose dissolution in the ionic liquid BmimAc. J Phys Chem B 125(29):8205–8218

Li Y, Wang J, Liu X, Zhang S (2018) Towards a molecular understanding of cellulose dissolution in ionic liquids: anion/cation effect, synergistic mechanism and physicochemical aspects. Chem Sci 9(17):4027–4043

Liang Y, Hawkins JE, Ries ME, Hine PJ (2021) Dissolution of cotton by 1-ethyl-3-methylimidazolium acetate studied with time–temperature superposition for three different fibre arrangements. Cellulose 28(2):715–727

Lovell CS, Walker A, Damion RA, Radhi A, Tanner SF, Budtova T, Ries ME (2010) Influence of cellulose on ion diffusivity in 1-ethyl-3-methyl-imidazolium acetate cellulose solutions. Biomacromol 11(11):2927–2935

Lu B, Xu A, Wang J (2014) Cation does matter: how cationic structure affects the dissolution of cellulose in ionic liquids. Green Chem 16(3):1326–1335

McLaughlin E (1959) Viscosity and self-diffusion in liquids. Trans Faraday Soc 55:28–38

Mezzetta A, Becherini S, Pretti C, Monni G, Casu V, Chiappe C, Guazzelli L (2019) Insights into the levulinate-based ionic liquid class: synthesis, cellulose dissolution evaluation and ecotoxicity assessment. New J Chem 43(33):13010–13019

Miao C, Hamad WY (2013) Cellulose reinforced polymer composites and nanocomposites: a critical review. Cellulose 20(5):2221–2262

Moulthrop JS, Swatloski RP, Moyna G, Rogers RD (2005) High-resolution 13C NMR studies of cellulose and cellulose oligomers in ionic liquid solutions. Chem Commun 12:1557–1559

Ocreto JB, Chen W-H, Rollon AP, Ong HC, Pétrissans A, Pétrissans M, De Luna MDG (2022) Ionic liquid dissolution utilized for biomass conversion into biofuels, value-added chemicals and advanced materials: a comprehensive review. Chem Eng J 445:136733

Olivier-Bourbigou H, Magna L, Morvan D (2010) Ionic liquids and catalysis: recent progress from knowledge to applications. Appl Catal A Gen 373(1–2):1–56

Quijada-Maldonado E, Van Der Boogaart S, Lijbers J, Meindersma G, De Haan A (2012) Experimental densities, dynamic viscosities and surface tensions of the ionic liquids series 1-ethyl-3-methylimidazolium acetate and dicyanamide and their binary and ternary mixtures with water and ethanol at T=(298.15 to 343.15 K). J Chem Thermodyn 51:51–58

Rabideau BD, Ismail AE (2015) Mechanisms of hydrogen bond formation between ionic liquids and cellulose and the influence of water content. Phys Chem Chem Phys 17(8):5767–5775

Reddy N, Yang Y (2005) Biofibers from agricultural byproducts for industrial applications. Trends Biotechnol 23(1):22–27

Ries ME, Radhi A, Keating AS, Parker O, Budtova T (2014) Diffusion of 1-ethyl-3-methyl-imidazolium acetate in glucose, cellobiose, and cellulose solutions. Biomacromol 15(2):609–617

Roy H, Rodgers M (2020) Absolute trends and accurate and precise gas-phase binding energies of 1-alkyl-3-methylimidazolium tetrafluoroborate ionic liquid clusters from combined independent and competitive TCID measurements. J Phys Chem A 124(49):10199–10215

Roy HA, Rodgers M (2021) 1-alkyl-3-methylimidazolium cation binding preferences in hexafluorophosphate ionic liquid clusters determined using competitive TCID measurements and theoretical calculations. Phys Chem Chem Phys 23(33):18145–18162

Seki S, Kobayashi T, Kobayashi Y, Takei K, Miyashiro H, Hayamizu K, Tsuzuki S, Mitsugi T, Umebayashi Y (2010) Effects of cation and anion on physical properties of room-temperature ionic liquids. J Mol Liq 152(1–3):9–13

Soykeabkaew N, Nishino T, Peijs T (2009) All-cellulose composites of regenerated cellulose fibres by surface selective dissolution. Compos Part A Appl Sci Manuf 40(4):321–328

Stejskal EO, Tanner JE (1965) Spin diffusion measurements: spin echoes in the presence of a time-dependent field gradient. J Chem Phys 42(1):288–292

Swatloski RP, Spear SK, Holbrey JD, Rogers RD (2002) Dissolution of cellose with ionic liquids. J Am Chem Soc 124(18):4974–4975

Tanpichai S, Boonmahitthisud A, Soykeabkaew N, Ongthip L (2022) Review of the recent developments in all-cellulose nanocomposites: properties and applications. Carbohydr Polym 286:119192

Tokuda H, Hayamizu K, Ishii K, Susan MABH, Watanabe M (2004) Physicochemical properties and structures of room temperature ionic liquids. 1. variation of anionic species. J Phys Chem B 108(42):16593–16600

Victoria A, Ries ME, Hine PJ (2022) Use of interleaved films to enhance the properties of all-cellulose composites. Compos Part A Appl Sci Manuf 160:107062

Vilaro P, Li K, Moyna G, Jiang H, Gurau G, Rogers RD (2024) Use of ionic liquids for hemp fiber degumming. ACS Sustain Chem Eng 12(34):12819–12826

Villar L, Pita M, Paez J, Sánchez PB (2023) Dissolution kinetics of cellulose in ionic solvents by polarized light microscopy. Cellulose. https://doi.org/10.1007/s10570-022-05036-0

Vitz J, Erdmenger T, Haensch C, Schubert US (2009) Extended dissolution studies of cellulose in imidazolium based ionic liquids. Green Chem 11(3):417–424

Wang Y, Voth GA (2006) Tail aggregation and domain diffusion in ionic liquids. J Phys Chem B 110(37):18601–18608

Wang S, Lu A, Zhang L (2016) Recent advances in regenerated cellulose materials. Prog Polym Sci 53:169–206

Xu A, Wang J, Wang H (2010) Effects of anionic structure and lithium salts addition on the dissolution of cellulose in

1-butyl-3-methylimidazolium-based ionic liquid solvent systems. Green Chem 12(2):268–275
Xu A, Wang J, Zhang Y, Chen Q (2012) Effect of alkyl chain length in anions on thermodynamic and surface properties of 1-butyl-3-methylimidazolium carboxylate ionic liquids. Ind Eng Chem Res 51(8):3458–3465
Xu A, Zhang Y, Lu W, Yao K, Xu H (2014) Effect of alkyl chain length in anion on dissolution of cellulose in 1-butyl-3-methylimidazolium carboxylate ionic liquids. J Mol Liq 197:211–214
Xu A, Cao L, Wang B, Ma J (2015) Dissolution behavior of cellulose in IL+ DMSO solvent: effect of alkyl length in imidazolium cation on cellulose dissolution. Adv Mater Sci Eng. https://doi.org/10.1155/2015/406470
Yadav A, Guha A, Pandey A, Pal M, Trivedi S, Pandey S (2018) Densities and dynamic viscosities of ionic liquids having 1-butyl-3-methylimidazolium cation with different anions and bis (trifluoromethylsulfonyl) imide anion with different cations in the temperature range (283.15 to 363.15) K. J Chem Thermodyn 116:67–75
Zhang H, Wu J, Zhang J, He J (2005) 1-allyl-3-methylimidazolium chloride room temperature ionic liquid: a new and powerful nonderivatizing solvent for cellulose. Macromolecules 38(20):8272–8277
Zhang J, Zhang H, Wu J, Zhang J, He J, Xiang J (2010) NMR spectroscopic studies of cellobiose solvation in EmimAc aimed to understand the dissolution mechanism of cellulose in ionic liquids. Phys Chem Chem Phys 12(8):1941–1947
Zhang Y, Xu A, Lu B, Li Z, Wang J (2015) Dissolution of cellulose in 1-allyl-3-methylimizodalium carboxylates at room temperature: a structure–property relationship study. Carbohydr Polym 117:666–672
Zhang J, Xu L, Yu J, Wu J, Zhang X, He J, Zhang J (2016) Understanding cellulose dissolution: effect of the cation and anion structure of ionic liquids on the solubility of cellulose. Sci China Chem 59:1421–1429
Zhang X, Ries ME, Hine PJ (2021) Time-temperature superposition of the dissolution of silk fibers in the ionic liquid 1-ethyl-3-methylimidazolium acetate. Biomacromol 22(3):1091–1101
Zhao Y, Gao S, Wang J, Tang J (2008) Aggregation of ionic liquids [C n mim] Br (n= 4, 6, 8, 10, 12) in D2O: a NMR study. J Phys Chem B 112(7):2031–2039
Zhao Y, Liu X, Wang J, Zhang S (2012) Effects of cationic structure on cellulose dissolution in ionic liquids: a molecular dynamics study. ChemPhysChem 13(13):3126–3133
Zhao Y, Liu X, Wang J, Zhang S (2013) Effects of anionic structure on the dissolution of cellulose in ionic liquids revealed by molecular simulation. Carbohydr Polym 94(2):723–730